
When Eyes Betray AI: Social Gaze Consistency as a Semantic Cue for AI-Generated Image Detection

Jihyeon Kim

School of Computer Engineering
Hoseo University
20220991@vision.hoseo.edu

Sohee Kim

School of Electronic Engineering
Soongsil University
soheekim@soongsil.ac.kr

Soosan Lee

School of Electronic Engineering
Soongsil University
susana0221@soongsil.ac.kr

Souhwan Jung

School of Electronic Engineering
Soongsil University
souhwanj@ssu.ac.kr

James Matthew Rehg

School of Computer Science
University of Illinois at Urbana-Champaign
jrehg@illinois.edu

Hyesong Choi

School of Electronic Engineering
Soongsil University
hyesong@ssu.ac.kr

Abstract

Recent generative models have largely closed the gap on low-level artifacts—pixel fingerprints, frequency anomalies, upsampling traces—particularly in person-centric and partial-edit settings where the manipulated region is small and surrounded by photometrically authentic content. We introduce Social Gaze Consistency, a high-level semantic cue defined as the mutual coherence of gaze direction, head-eye alignment, and pupil placement between interacting individuals, and show that it constitutes a previously underutilized detection axis orthogonal to existing low-level paradigms. We instantiate this insight through three coupled mechanisms: (i) a controlled diagnostic dataset with region-specific perturbations of gaze-consistent imagery, where strict pair-level grouping forecloses generator-fingerprint memorization as an optimization-time shortcut rather than relying on augmentation; (ii) Block-Compositional Caption Supervision, which holds a single 5-block reasoning skeleton invariant across 1,250 macro-combined captions, decoupling reasoning consistency from surface diversity; (iii) Cross-architecture validation showing the same supervision improves a vision-language backbone (FakeVLM) by +3.7 pp on the COCOAI Interaction subset (balanced accuracy 67.8 \rightarrow 71.5) and +1.3 pp on the COCOAI Person subset (83.0 \rightarrow 84.3), with consistent gains on a vision-only backbone (Effort), evidencing a backbone-agnostic cue. Real- and fake-class recalls rise simultaneously, ruling out a “predict-all-fake” artifact. A four-step mechanistic account—paired-edit shortcut blocking, hard-to-easy difficulty transfer, CLIP prior preservation, and diffusion-family shared spectral weakness in periocular structure—explains why training on a single inpainter (FLUX.1-Fill) transfers to multi-generator suites. We will release the code upon acceptance to facilitate reproducibility.

1 Introduction

The trajectory of modern generative models—Stable Diffusion 3 [9], FLUX.1, DALL·E 3 [1], Midjourney v6—has progressively dismantled the low-level signals upon which the dominant lineage of AI-generated content (AIGC) detectors [31, 25, 30, 34] was built. Frequency-domain anomalies [10], neighboring-pixel relationships introduced by upsampling [8], characteristic skin-texture smoothing, and finger-count irregularities have all been substantially mitigated by successive model releases. The empirical consequence is striking: detectors such as NPR [30], UnivFD [25], and AIDE [34], which posted near-saturated accuracy on prior benchmarks, collapse to near-chance levels on contemporary multi-generator suites that involve human subjects (Section 4.3). This is not a mere distributional shift; it is the partial exhaustion of a cue space.

Compounding this, the threat surface itself has broadened. Beyond fully synthesized imagery, *partial-edit fakes*—in which a localized region of a real photograph is regenerated by an inpainting model [22, 24]—now constitute a practically significant attack vector spanning identity manipulation, social-media misinformation, and targeted facial-expression edits. Such fakes inherit the photometric statistics of authentic imagery everywhere except a small region, evading detectors that rely on globally distributed cues.

We argue that detection cues lie on at least two axes. The low-level axis comprises pixel statistics, frequency residuals, and architectural fingerprints—the territory progressively reclaimed by generators. The high-level semantic-consistency axis comprises socially meaningful relations between depicted entities [4]: the geometric coherence of mutual gaze, the alignment of head pose with eye direction, and the plausibility of attentional targets in multi-person scenes. The standard denoising diffusion objective does not explicitly enforce these higher-order relations: nothing penalizes a generated face whose eyes drift fractionally off the partner’s gaze target while remaining locally photorealistic.

Earlier work in social-interaction recognition (notably LAEO-Net [23]) established mutual gaze as a primary signal for video-based interaction parsing. We transpose this insight into a previously unexamined setting: single-image AIGC detection, where mutual gaze becomes a falsifiable geometric prediction rather than an action-recognition target.

Person-centric and interaction-centric content constitutes the weakest territory for the *current generation* of detectors—precisely where a semantic cue should help the most. On the multi-person interaction subset we curate from MS COCOAI [29], the dominant low-level detectors collapse to near-random performance (BA, %): AIDE [34] (48.7), NPR [30] (51.5), and UnivFD [25] (50.0). Even shortcut-robust detectors such as Effort [33] (59.0) and SIDA-13B [15] (60.9) remain stuck in the 50–60 range, with the same pattern persisting on the broader person-centric subset—motivating an orthogonal, semantically grounded detection axis.

We make three primary contributions, supported by a *Custom Gaze* diagnostic dataset constructed for these experiments.

(C1) A new cue. We introduce *Social Gaze Consistency* as a semantic detection axis distinct from low-level paradigms and prior single-person periocular forensics, with cross-generator transferability substantiated by a four-step mechanism.

(C2) A supervision design. We propose *Block-Compositional Caption Supervision*, whose macro-pool sampling produces 1,250 unique captions with an invariant reasoning skeleton from only 20 macro-pool entries.

(C3) Cross-architecture validation. The same supervision improves FakeVLM by +3.7 pp on the COCOAI interaction-centric subset (BA 67.8 → 71.5) and +1.3 pp on the person-centric subset (83.0 → 84.3), with consistent gains on Effort, evidencing an anatomically grounded, generator-agnostic signal.

The supporting Custom Gaze dataset—46,830 paired real/fake images with region-specific perturbations of gaze-consistent imagery (Appendix A)—underpins all three contributions through pair-level identity preservation that forecloses generator-fingerprint memorization.

2 Related Work

2.1 Vision-Language Detectors

The emergence of large multimodal models (LMMs) such as LLaVA [19, 20] has enabled fake detectors that produce explanatory natural-language output rather than binary scores. The decisive empirical observation comes from FakeVLM [32]: fine-tuning LLaVA-v1.5 on FakeClue (an explanation corpus of $\approx 104\text{K}$ AI-generated images paired with free-form captions describing visible synthesis artifacts) and switching the output head from a linear classifier to free-form text yields a +2.7 pp gain on LOKI [36]—a controlled isolation of how supervision *form* alone shapes detection performance. SIDA [15] extends this paradigm with a 13B-parameter LISA backbone and adds tampered-region localization. This lineage situates explanatory generation as a *learning signal* rather than post-hoc interpretation: by requiring the model to articulate *why* an image is fake during training, optimization is forced to internalize discriminative features at the conceptual level rather than at pixel statistics.

Our work refines this lineage at a finer granularity. Where FakeVLM establishes that *explanatory generation* (vs. binary classification) helps, we ask the next-level question: *which structural form* of explanation maximizes detection signal. We isolate the effect of injecting a fixed reasoning skeleton into supervision, decoupling reasoning consistency from raw output diversity.

2.2 Mutual Gaze in Recognition and Periocular Cues in Forensics

Mutual gaze in social-interaction recognition. LAEO-Net [23] introduced a three-branch CNN for “people looking at each other” detection in video, demonstrating that mutual gaze geometry is a high-information signal for social-interaction parsing. OI Mutual Gaze [7] released the first large-scale image-level mutual-gaze dataset with binary annotations on 29.2K Open Images. A complementary research line on gaze following [28] and attention target detection [5] infers *where* a person is looking from a single image or video, supplying the geometric primitive (head \rightarrow attentional target) whose multi-person consistency our forensic cue exploits. Foundational gaze-estimation backbones [16, 37] further establish that head-pose and pupil-direction estimation have reached sufficient maturity for downstream forensic consumption.

Eye and gaze cues in deepfake forensics. A separate lineage exploits eye-region cues for deepfake detection: eye-blinking inconsistency [18] for first-generation GAN deepfakes, and pupil-shape irregularities [12] and iris-region forensics [14] for anatomically inconsistent ocular structure. These approaches all operate at the *single-person* level, exploiting intra-face anatomical priors.

Our positioning. Unlike LAEO-Net and OI Mutual Gaze, which use mutual gaze as an action-recognition or social-interaction *target*, we treat it as a *falsifiable forensic prediction*—a relation that authentic photographs satisfy by construction and that contemporary inpainting models systematically violate at the eye region. Unlike single-person eye-cue detectors, which exploit *intra-face* anatomical priors, our cue is fundamentally *inter-person*: the geometric coherence of two interacting individuals’ gaze vectors with their respective head poses.

3 Method

We formalize a person-centric AIGC detection problem and present three coupled components (Figure 1): (i) a paired-edit data construction that isolates the gaze cue from confounding generative fingerprints; (ii) a Block-Compositional Caption schema that injects a reasoning skeleton into supervision while preserving surface diversity; and (iii) a mixed fine-tuning protocol with balanced-accuracy checkpoint selection.

3.1 Problem Formulation

A detector outputs both a binary authenticity label (1=real, 0=fake) and a natural-language explanation $c \in \mathcal{T}$; following FakeVLM, we exploit \mathcal{T} as a supervision channel rather than as post-hoc interpretation.

We posit a two-axis cue decomposition: φ_{low} captures low-level statistics (frequency, pixel residuals, upsampling traces) and φ_{high} captures semantic-consistency descriptors (gaze geometry, head-eye

alignment, attentional targets). Within the person-centric subdomain under partial-edit attacks, we put forward the working hypothesis

$$I(Y; \varphi_{\text{high}}(x)) > I(Y; \varphi_{\text{low}}(x)), \quad (\text{H1})$$

tested behaviorally via downstream accuracy on partial-edit and interaction-centric subsets.

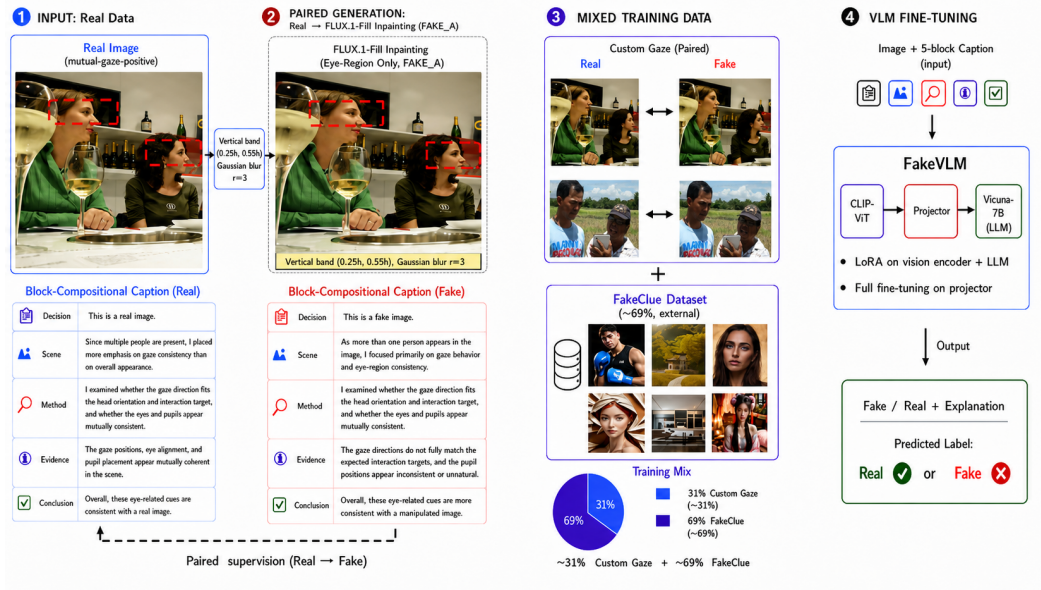


Figure 1: Custom Gaze construction and Block-Compositional Caption Supervision. Only the eye region is regenerated by FLUX.1-Fill; the paired real-fake samples share an invariant 5-block reasoning skeleton (Decision \rightarrow Scene \rightarrow Method \rightarrow Evidence \rightarrow Conclusion) with surface variation across 1,250 macro-combined captions.

3.2 Custom Gaze Dataset Construction

Our dataset construction is governed by a single design principle: pair-level identity preservation. Each fake image shares base identity, scene, lighting, and global composition with a corresponding real image, differing only within a localized eye region. This structure enables shortcut blocking during learning (cf. §4.4, M1): paired supervision forecloses memorizing FLUX-specific fingerprints.

Real source. Our real source is the mutual-gaze-positive subset of OI Mutual Gaze [7] (23,415 mutual-gaze-positive image-pairs derived from 8,972 retained source images via multi-bbox unpacking; (details in Appendix A.1); each retained image carries two face bounding boxes $(x_{\min}, y_{\min}, x_{\max}, y_{\max})$ for participants A and B.

Eye-region masking and inpainting. Given a face bounding box, we compute the eye-region mask M_{eye} via

$$M_{\text{eye}} = \{(i, j) : y_{\min} + 0.25h \leq i \leq y_{\min} + 0.55h \text{ and } x_{\min} + 0.05w \leq j \leq x_{\max} - 0.05w\} \quad (1)$$

where $h \triangleq y_{\max} - y_{\min}$ and $w \triangleq x_{\max} - x_{\min}$. The vertical band $[0.25h, 0.55h]$ empirically isolates the eye region across pose variations while excluding nose, mouth, hair, and background, and a Gaussian blur of radius 3 softens mask boundaries. We employ FLUX.1-Fill-dev [2] (a 12B rectified flow transformer; abbreviated FLUX.1-Fill in subsequent text) in bfloat16 at 20 inference steps, guidance scale 25 (see Appendix A.1 for full pipeline); images are resized to max side 1024 px and aligned to a 16-pixel grid per FLUX requirement.

Final composition. Custom Gaze comprises 46,830 images split 8 : 1 : 1 (train : val : test) with stratification and *pair-level grouping* to prevent leakage; the test split is the partial-edit hard-fake benchmark used throughout. The datasheet is in Appendix A.

3.3 Block-Compositional Caption Supervision

Recent advances in instruction-tuned LLMs [19, 32] have established that *what the model is asked to output* is at least as consequential as *what it is asked to predict*. Table 6 of Wen et al. [32] isolates this effect: switching the output head from a linear classifier to free-form text yields +2.7 pp on LOKI. We hypothesize a finer claim: the *structural depth* of the requested output, when properly compositionally encoded, induces detector behavior qualitatively different from either binary classification or unstructured generation.

We instantiate this through a 5-tuple caption schema $c = (p_1, p_2, p_3, p_4, p_5)$ corresponding to Decision (label header), Scene (multi-person context), Method (cue-type declaration: gaze-based reasoning), Evidence (gaze-geometric observation), and Conclusion (verdict synthesis). Position p_1 is deterministic given the label ($p_1(\text{real}) = \text{“This is a real image.”}$; $p_1(\text{fake}) = \text{“This is a fake image.”}$), while positions p_2 through p_5 are populated by sampling from per-position macro pools of cardinality 5, yielding $|C| = 1 \times 5^4 \times 2 = 1,250$ unique captions distributed approximately uniformly across 18,732 training samples per label. The *reasoning skeleton* (Scene \rightarrow Method \rightarrow Evidence \rightarrow Conclusion) is invariant across all 1,250 captions; only the surface lexicalization of each block varies.

Why compositional, not free-form? A natural alternative is to delegate caption generation to a stronger LMM (e.g., GPT-4o, Qwen2-VL-72B), as FakeVLM does for its FakeClue corpus. This works for general AIGC detection but not for gaze: in qualitative pilot studies, off-the-shelf LMMs defaulted to texture-based reasoning even when explicitly prompted toward gaze cues, failing to instill consistent gaze-centric reasoning. Our schema resolves this through a single reasoning path \times 1,250 surface variants design choice, which simultaneously achieves (i) mode collapse prevention, with unique output ratio ranging 0.93–0.97 across post-warmup training (mean 0.94; 0.93 at the deployed step 1,650; 0.96 over the last 50 evaluations; full diagnostics in Appendix C.2); (ii) reasoning coherence, with TOP1_TEMPLATE_RATIO stabilizing at 0.52–0.53; and (iii) annotation cost reduction from $\mathcal{O}(N)$ per-sample human authoring to a constant 20 macro-pool entries (4 positions \times 5 variants), which yield tens of thousands of captions via combinatorial sampling.

Training objective. The supervision channel is realized through standard token-level cross-entropy on the assistant’s response tokens (with question tokens masked)

$$\mathcal{L}_{\text{caption}}(\theta) = -\mathbb{E}_{(x,c)\sim\mathcal{D}} \left[\sum_{t=1}^{|c|} \log p_{\theta}(c_t \mid c_{<t}, x) \right], \quad (2)$$

with the question turn (“Does the image look real/fake?”) masked from the loss. At inference, we extract the label via a deterministic regex matching the prefix `This is a (real|fake) image.` over p_1 , requiring no learned classification head.

Mix composition. To prevent person-only training from inducing distributional collapse on non-person categories, we mix the Custom Gaze dataset (46,830 samples = 23,415 paired images across the train/val/test splits, with the pair-level grouping of §3.2 ensuring that val/test pairs are excluded from gradient updates) with the 104,343-sample FakeClue training set [32], yielding 151,173 total samples (\approx 31% gaze, \approx 69% FakeClue). FakeClue captions are retained in their original free-form form, providing complementary texture-centric supervision.

3.4 Mixed Fine-Tuning with Balanced-Accuracy Checkpointing

Trainable parameters. We adopt FakeVLM (LLaVA-v1.5 + Vicuna-v1.5-7B + CLIP-ViT-L/14-336) as our base and apply parameter-efficient fine-tuning differentially across three modules:

Table 1: Adaptation configuration: LoRA on vision encoder and LLM; full fine-tuning on the projector as the cross-modal bottleneck.

Module	Adaptation
Vision encoder (CLIP-ViT)	LoRA, all attention and MLP linear layers
Vision-language projector	Full fine-tuning (<code>modules_to_save</code>)
LLM (Vicuna-7B)	LoRA, all attention and MLP linear layers

LoRA [13] hyperparameters: rank $r=16$; scaling $\alpha=32$; dropout 0.05; bias none. Trainable parameters constitute approximately 0.6% of the base model ($\sim 45\text{M}$ of $\sim 7\text{B}$). The asymmetry reflects that the projector is the *modality bridge* where gaze-cue integration most directly requires reweighting of cross-modal correspondences.

Optimization. We optimize with AdamW [21] ($\beta = (0.9, 0.999)$, $\varepsilon = 10^{-8}$, $\lambda=0$) at peak learning rate 2×10^{-5} under a cosine schedule with warmup ratio 0.03. The effective batch size is 32 (per-device 1, gradient accumulation 4, 8 GPUs) on RTX A6000s with DeepSpeed ZeRO-2 [27] and bfloat16 precision. Training proceeds for 2 epochs (7,558 steps), with sequence maximum length 1,024 tokens and random seed fixed to 42.

Balanced-accuracy checkpoint selection. We select the deployed checkpoint by balanced accuracy rather than validation loss. With sensitivity $\text{TPR} \triangleq \text{TP}/(\text{TP} + \text{FN})$ and specificity $\text{TNR} \triangleq \text{TN}/(\text{TN} + \text{FP})$, balanced accuracy is $\text{BA} = (\text{TPR} + \text{TNR})/2$ [3]. For explanatory generative detectors, validation loss and BA decouple: a model can reduce token-level loss by drifting toward template uniformity while sacrificing class-balanced classification competence. Empirically, our loss minimum occurs at step 2,850 (loss = 0.2252) while BA peaks at step 1,650 (BA = 0.9990)—a gap of 1,200 steps. We therefore select

$$\theta^* = \arg \max_{\theta_t} \text{BA}(\theta_t; \mathcal{D}_{\text{dev}}), \quad (3)$$

with \mathcal{D}_{dev} a held-out 970-sample mixture (470 Custom Gaze + 500 FakeClue test samples), evaluated every 50 steps. We refer to the resulting checkpoint as MIX1650 and use it as the deployed model throughout the experiments.

4 Experiments

4.1 Experimental Protocol

Evaluation suites. We evaluate on three benchmarks chosen to triangulate distinct failure modes of multi-generator AIGC: Custom Gaze (partial-edit hard fakes), COCOAI Person (single-person AIGC across five generators) [29], and COCOAI Interaction \star (multi-person interaction; our *core evidence* benchmark) [29]. Per-benchmark construction—caption-keyword filters, balancing protocol, caption schema, and representative example images—is detailed in Appendix A.2.

Table 2: Evaluation benchmarks spanning partial-edit hard fakes, person-centric AIGC, and multi-person interaction fakes.

#	Dataset	N	Real:Fake	Probes
1	Custom Gaze (test)	4,684	2,342:2,342	partial-edit hard fake
2	COCOAI Person	15,720	2,620:13,100	person-centric AIGC (5 generators)
3	COCOAI Interaction \star	198	33:165	multi-person interaction (core)

Both COCOAI subsets exhibit a 1:5 real-to-fake imbalance under which plain accuracy is uninformative; we therefore report balanced accuracy (BA), macro-F1, and Matthews Correlation Coefficient (MCC), and the unweighted arithmetic mean across the three benchmarks—MCC, which penalizes majority-class collapse, serves as the strictest single indicator of genuine discrimination. All inference runs on a single RTX 4080 SUPER (16 GB); FakeVLM variants are loaded in 4-bit NF4 quantization [6] and external baselines at their authors’ recommended precision, with greedy decoding ($\text{MAX_NEW_TOKENS} = 64$, SDPA attention) and labels extracted via regex over the first decision keyword.

Baselines. We compare against seven prior systems spanning low-level forensics and LMM-based detection: FakeVLM origin [32], Effort [33], NPR [30], UnivFD [25], AIDE [34], SAFE [17], and SIDA-13B [15], the most direct LMM-based competitor. Per-baseline configurations and the SIDA three-class binarization protocol is detailed in Appendix B.

Table 3: Per-dataset balanced metrics for FakeVLM origin and our BA-best checkpoint, reported as mean \pm std over 3 seeds {42, 47, 53}. Best per column in bold.

Method	COCOAI_Inter			COCOAI_Person			Custom Gaze		
	BA	F1	MCC	BA	F1	MCC	BA	F1	MCC
FakeVLM origin	68.3 \pm 0.4	64.9 \pm 0.8	31.6 \pm 1.2	83.1 \pm 0.1	78.4 \pm 0.2	58.4 \pm 0.3	86.5 \pm 0.2	86.3 \pm 0.3	75.7 \pm 0.4
Ours (mix1650)	71.1\pm0.3	71.9\pm0.2	43.8\pm0.3	84.3\pm0.1	83.8\pm0.1	67.6\pm0.2	99.9\pm0.0	99.9\pm0.0	99.8\pm0.1

4.2 Main Result: FakeVLM Origin vs. Ours

The pattern admits a clean interpretation. In-distribution (Custom Gaze) saturates at the practical ceiling: BA 86.4 \rightarrow 99.9 (+13.5 pp), macro-F1 +13.7 pp, MCC +24.4 pp. Cross-distribution but person-centric (COCOAI Person, single-person AIGC across five generators including DALL·E 3, SDXL, SD3, SD2.1, Midjourney v6) shows consistent moderate gains: BA +1.3 pp, macro-F1 +5.6 pp, MCC +9.6 pp. Cross-distribution and cross-task (COCOAI Interaction)—the diagnostic case, multi-person fully-synthesized AIGC drawn from neither partial edits nor single-person regimes—improves by +3.7 pp BA, +7.5 pp macro-F1, and +13.3 pp MCC; the macro-F1 and MCC margins exceed the BA margin by a factor of two-to-four, the canonical signature of recovering minority-class structure rather than inflating the majority class. The mean improvement is +6.1 pp BA, +8.9 pp macro-F1, and +15.7 pp MCC.

Table 4: Confusion-matrix dissection on COCOAI Interaction ($n = 198$): +17 fake recovery with near-zero real-class perturbation.

	Origin	Ours	Δ
WRONG_REAL (missed fakes / 165)	31	14	-17
RIGHT_FAKE (caught fakes / 165)	134	151	+17
RIGHT_REAL (real correctly classified / 33)	18	17	-1
WRONG_FAKE (real misclassified / 33)	15	16	+1

Confusion-matrix dissection on COCOAI Interaction ($n = 198$, 33 real / 165 fake): The +17-fake recovery is achieved with a near-zero perturbation of real classification (-1 RIGHT_REAL, $+1$ WRONG_FAKE), refuting the alternative hypothesis that the gain is a calibration drift toward predicting “fake”: were that the case, real-class accuracy would degrade in proportion to the fake-class gain. The signature—substantial fake recovery without commensurate real degradation—is the hallmark of genuine cue acquisition. The gain profile across the three benchmarks (in-distribution saturation, MCC-driven minority recovery on interaction fakes, modest consistent gains on COCOAI Person) is itself diagnostic of a domain-targeted intervention: the gaze-consistency cue maximally lifts performance on the multi-person interaction regime its theoretical motivation explicitly addresses.

4.3 External Baseline Comparison

Table 5: External baseline comparison: balanced metrics across the three benchmarks. Best per column in bold. *Top block*: low-level / classifier baselines and SIDA. *Bottom block*: FakeVLM family (origin vs. ours, mix1650).

Model	COCOAI_I			COCOAI_P			Custom Gaze		
	BA	macro-F1	MCC	BA	macro-F1	MCC	BA	macro-F1	MCC
AIDE	48.7	28.7	-2.2	47.0	27.7	-5.6	44.0	31.5	-23.0
SAFE	46.9	13.5	-22.5	50.0	14.3	1.1	50.0	33.3	1.4
NPR (nores+tta)	51.5	17.5	7.1	50.6	17.8	2.8	28.7	22.6	-51.4
UnivFD	50.0	14.2	0.0	50.0	14.6	0.8	50.7	35.0	8.0
SIDA-13B (LMM)	60.9	57.1	17.6	68.2	66.0	32.7	83.3	82.9	69.9
FakeVLM origin	67.8	64.6	30.8	83.0	78.2	58.1	86.4	86.2	75.5
Ours (mix1650)	71.5	72.1	44.1	84.3	83.8	67.7	99.9	99.9	99.9

The five low-level detectors (AIDE, SAFE, Effort, NPR, UnivFD) collapse to $BA \leq 59$ on Interaction and ≤ 71 on Person, with NPR’s and UnivFD’s MCC at-or-near zero across all three benchmarks—the low-level paradigm scarcely beats chance against contemporary multi-generator person-centric content (per-model breakdown and qualitative limitation analysis in Appendix B). SIDA-13B, the most direct LMM competitor at 13B parameters, attains a respectable mean BA of 70.8 but is surpassed by our 7B model by +14.4 pp on unweighted mean BA, +16.6 pp on macro-F1, and +30.5 pp on MCC. Two findings follow. Within the LMM-detector family, supervision design dominates parameter count: a 7B model with deliberately constructed gaze supervision exceeds a 13B model trained on conventional fake-detection corpora across every metric on every benchmark. The +6.1 pp jump from FakeVLM origin (mean BA 79.0) to ours (mean BA 85.2) is achieved under identical backbone and inference protocol, isolating data-and-caption design as the locus of the gain.

The advantage widens under MCC. Ours achieves mean MCC 70.5, the only model in the comparison to clear the 70 mark; SIDA reaches 40.0 ($\Delta -30.5$ pp), FakeVLM origin 54.8 ($\Delta -15.7$ pp), and the five low-level detectors all fall below 18, three of them below zero. Among the eight systems compared, only ours produces predictions whose joint confusion structure clears the majority-class baseline by a non-trivial margin on every benchmark.

4.4 Cross-Architecture Generalization

We test whether the gaze cue is FakeVLM-specific or transferable to other visual backbones. We fine-tune Effort [33]—a vision-only CLIP-ViT-L/14 detector with SVD-residual self-attention that shares only the CLIP backbone with FakeVLM—on the 37,464-sample Custom Gaze training split under a DeepfakeBench [35]-style recipe. Because Effort emits a scalar score rather than a caption, supervision necessarily reduces to label level; what transfers is therefore the paired-edit data structure and the gaze cue itself, not the caption schema. Table 6 reports this canonical variant (Ours, Effort gaze-FT) alongside Effort origin, while a parallel UFD-style recipe exhibits the same in-distribution saturation and same-direction cross-distribution transfer (recipe details and per-benchmark numbers in Appendix B.2).

Table 6: Effort family: cross-architecture validation on a vision-only Effort backbone (CLIP-ViT-L/14 with SVD-residual self-attention; shares only the CLIP backbone with FakeVLM). *Origin*: Effort released checkpoint; *Ours*, *Effort gaze-FT*: Effort fine-tuned on the 37,464-sample Custom Gaze training split under a DeepfakeBench-style recipe (label-level supervision; §4.4, Appendix B.2)

Model	COCOAI_I			COCOAI_P			Custom Gaze		
	BA	macro-F1	MCC	BA	macro-F1	MCC	BA	macro-F1	MCC
Effort origin	59.0	49.9	13.5	70.6	58.2	30.8	50.9	36.1	6.7
Ours (Effort, gaze-FT)	62.4	58.1	20.0	75.2	66.2	39.5	99.9	99.9	99.9

Effort gaze-FT saturates Custom Gaze at the same ceiling as FakeVLM (+49.0 pp BA, +93.2 pp MCC; Table 5) despite a fundamentally different architecture, and on the COCOAI subsets reproduces FakeVLM’s minority-class-recovery signature with macro-F1 and MCC gains exceeding BA gains on every benchmark.

We synthesize the empirical evidence into a four-step mechanistic account:

(M1) Paired-edit shortcut blocking. All 18,732 training pairs (Custom Gaze train split; 23,415 across the full dataset) share base identity, scene, and lighting; the only intra-pair difference is the eye region. The detector cannot reduce loss by latching onto FLUX-specific global fingerprints; the optimization landscape forces anatomically grounded eye-region features.

(M2) CLIP prior preservation. Both Effort (SVD-residual) and our LoRA configuration preserve the bulk of CLIP’s pretrained representations [26]. Cross-generator generalization is inherited from CLIP’s 400M-pair pretraining—FLUX, SDXL, SD3, and DALL·E imagery occupy approximately commensurable feature regions—rather than learned by the detector in any narrow sense.

The decisive empirical signature is the cross-architecture pattern itself: a non-LMM vision-only detector, trained on identical supervision, exhibits the same in-distribution saturation and the same direction of cross-distribution transfer. Were the cue an architecture-specific phenomenon, this replication would not occur.

5 Ablation Study

Holding backbone, LoRA configuration, training mixture, optimizer, and checkpoint-selection protocol constant, we compare two endpoints of caption-supervision depth: the proposed five-sentence Block-Compositional schema (full reasoning skeleton, 1,250 unique captions) versus a one-sentence decision-only schema (minimal label-statement, 2 unique captions). This A-vs-B contrast isolates the marginal contribution of the reasoning skeleton.

Table 7: Supervision depth variants: 5-block schema (1,250 captions) vs. decision-only baseline (2 captions) isolating the reasoning skeleton.

Variant	Caption sentences	Positions used	Unique captions
A. Mix (proposed)	5	$p_1 + p_2 + p_3 + p_4 + p_5$	1,250
B. Decision-only	1	p_1	2

Table 8: Caption design ablation. Each variant evaluated at its own BA-best checkpoint, selected on the same 970-sample dev mixture as the deployed model. The COCOAI Inter / Person columns report fake-class accuracy on the deepfake-only subsets ($n=270$ for Interaction and $n=1,000$ for Person), chosen so that the caption-design contrast is read directly off fake-class detection performance without dilution from the real class; the Custom Gaze column reports balanced accuracy on the 4,684-sample 1:1 split. Mean is the unweighted arithmetic mean across the three displayed benchmarks.

Variant	COCOAI_I	COCOAI_P	Custom Gaze	Mean
A. Mix (5-sent, st1650)	84.3	88.1	99.9	90.7
B. Decision-only (1-sent, st1500)	81.4	90.7	99.9	90.6

At first glance the result is paradoxical: the means differ by only +0.1 pp ($A = 90.7$ vs. $B = 90.6$), yet the per-benchmark distribution is non-trivial. A leads by +2.9 pp on COCOAI Interaction (our core-evidence benchmark), B leads by +2.6 pp on COCOAI Person, and both saturate on Custom Gaze. The opposite-sign deltas cancel in the mean.

Interpretation. Reasoning depth is *not* a uniform enhancer; it is a domain-targeted lever whose effect manifests only where the reasoning aligns with the benchmark’s semantic structure. On Custom Gaze, the base classification signal saturates without any reasoning. On COCOAI Person, a five-sentence rationale built around multi-person gaze geometry over-specializes for single-person fakes. Only on multi-person interaction fakes—where the gaze skeleton aligns by design—does additional reasoning depth produce a positive gain. The opposite-sign deltas are consistent with a domain-targeted interpretation, and are invisible in the aggregate Mean. Card-level failure analysis, mode-collapse diagnostics, and the inference-time behavior of variant B (confirming that reasoning capacity is acquired through supervision) appear in Appendices C, D, and E.3.

6 Discussion and Limitations

Our results admit a two-axis cue decomposition reading: gaze geometry, head–eye alignment, and attentional plausibility form a high-level semantic-consistency axis complementary to the low-level paradigms (NPR, UnivFD, AIDE, Effort origin) whose territory contemporary generators progressively reclaim. The scope is deliberately person-centric; we delineate four limitations—(L1) domain specialization, (L2) card over-trust, (L3) single-generator (FLUX.1-Fill) construction, and (L4) face-detection dependency at training time—and three future directions (video extension, multi-cue composition, principled card gating) in Appendix E.

7 Conclusion

We have argued that AI-generated image detection, in the current generator regime, requires an additional cue axis beyond the low-level paradigm—one grounded in social-semantic consistency rather than pixel statistics. Operationalizing this argument through Social Gaze Consistency, Block-Compositional Caption Supervision, and the Custom Gaze paired-edit dataset, we have demonstrated,

on three person-centric benchmarks: (i) on the COCOAI benchmark, balanced-accuracy gains of +3.7 pp on the interaction-centric subset (67.8 \rightarrow 71.5) and +1.3 pp on the person-centric subset (83.0 \rightarrow 84.3) over FakeVLM origin, with corresponding leads of +10.6 pp and +16.1 pp BA over a 13B LMM competitor (SIDA-13B), achieved with a 7B backbone via supervision design alone; (ii) cross-architecture transfer to a vision-only Effort backbone, with parallel in-distribution saturation (+49.0 pp BA on Custom Gaze) and consistent same-direction cross-distribution gains on every metric, confirming the cue’s architecture-agnostic nature; (iii) a domain-targeted reasoning-depth effect isolable only by examining benchmark-specific rather than averaged behavior—a +2.9 pp lift on multi-person interaction fakes that fully cancels in the mean against the opposite-sign delta on single-person fakes; and (iv) a four-step mechanistic account—paired-edit shortcut blocking, hard-to-easy difficulty transfer, CLIP prior preservation, and diffusion-family shared spectral weakness in periocular structure—explaining why single-generator inpainting supervision transfers to multi-generator full-image evaluation across architectures. We expect the semantic-consistency cue space to become increasingly central as low-level artifacts continue to recede.

References

- [1] James Betker, Gabriel Goh, Li Jing, Tim Brooks, Jianfeng Wang, Linjie Li, Long Ouyang, Juntang Zhuang, Joyce Lee, Yufei Guo, Wesam Manassra, Prafulla Dhariwal, Casey Chu, Yunxin Jiao, and Aditya Ramesh. Improving image generation with better captions. Technical report, OpenAI, 2023.
- [2] Black Forest Labs. Flux.1 fill [dev]. Technical report, Black Forest Labs, 2024.
- [3] K. H. Brodersen et al. The balanced accuracy and its posterior distribution. In *International Conference on Pattern Recognition*, 2010.
- [4] X. Cao et al. Socialgesture: Delving into multi-person gesture understanding. In *Proceedings of the IEEE/CVF Conference on Computer Vision and Pattern Recognition*, 2025. arXiv:2504.02244.
- [5] Eunji Chong, Yongxin Wang, Nataniel Ruiz, and James M. Rehg. Detecting attended visual targets in video. In *Proceedings of the IEEE/CVF Conference on Computer Vision and Pattern Recognition*, 2020.
- [6] T. Dettmers et al. Qlora: Efficient finetuning of quantized llms. In *Advances in Neural Information Processing Systems*, 2023.
- [7] B. Doosti et al. Boosting image-based mutual gaze detection using pseudo 3d gaze. In *AAAI Conference on Artificial Intelligence*, 2021. arXiv:2010.07811.
- [8] Ricard Durall, Margret Keuper, and Janis Keuper. Watch your up-convolution: CNN based generative deep neural networks are failing to reproduce spectral distributions. In *Proceedings of the IEEE/CVF Conference on Computer Vision and Pattern Recognition*, 2020.
- [9] Patrick Esser, Sumith Kulal, Andreas Blattmann, Rahim Entezari, Jonas Müller, Harry Saini, Yam Levi, Dominik Lorenz, Axel Sauer, Frederic Boesel, Dustin Podell, Tim Dockhorn, Zion English, and Robin Rombach. Scaling rectified flow transformers for high-resolution image synthesis. In *International Conference on Machine Learning*, 2024.
- [10] Joel Frank, Thorsten Eisenhofer, Lea Schönherr, Asja Fischer, Dorothea Kolossa, and Thorsten Holz. Leveraging frequency analysis for deep fake image recognition. In *International Conference on Machine Learning*, 2020.
- [11] T. Gebu, J. Morgenstern, B. Vecchione, J. W. Vaughan, H. Wallach, H. D. Iii, and K. Crawford. Datasheets for datasets. *Communications of the ACM*, 64(12):86–92, 2021.
- [12] H. Guo, S. Hu, X. Wang, M.-C. Chang, and S. Lyu. Eyes tell all: Irregular pupil shapes reveal GAN-generated faces. In *IEEE International Conference on Acoustics, Speech and Signal Processing (ICASSP)*, 2022.
- [13] E. J. Hu et al. Lora: Low-rank adaptation of large language models. In *International Conference on Learning Representations*, 2022. arXiv:2106.09685.
- [14] Shu Hu, Yuezun Li, and Siwei Lyu. Exposing GAN-generated faces using inconsistent corneal specular highlights. In *IEEE International Conference on Acoustics, Speech and Signal Processing (ICASSP)*, pages 2500–2504, 2021.

- [15] Z. Huang et al. Sida: Social media image deepfake detection, localization and explanation with large multimodal model. In *Proceedings of the IEEE/CVF Conference on Computer Vision and Pattern Recognition*, 2025. arXiv:2412.04292.
- [16] P. Kellnhofer, A. Recasens, S. Stent, W. Matusik, and A. Torralba. Gaze360: Physically unconstrained gaze estimation in the wild. In *Proceedings of the IEEE/CVF International Conference on Computer Vision*, 2019.
- [17] Ouxiang Li, Jiayin Cai, Yanbin Hao, Xiaolong Jiang, Yao Hu, and Fuli Feng. Improving synthetic image detection towards generalization: An image transformation perspectives. *arXiv preprint arXiv:2408.06741*, 2024.
- [18] Y. Li, M.-C. Chang, and S. Lyu. In *ictu oculi*: Exposing ai generated fake face videos by detecting eye blinking. In *IEEE International Workshop on Information Forensics and Security (WIFS)*, 2018.
- [19] H. Liu et al. Visual instruction tuning. In *Advances in Neural Information Processing Systems*, 2023. Oral, arXiv:2304.08485.
- [20] H. Liu et al. Improved baselines with visual instruction tuning. In *Proceedings of the IEEE/CVF Conference on Computer Vision and Pattern Recognition*, 2024. arXiv:2310.03744.
- [21] Ilya Loshchilov and Frank Hutter. Decoupled weight decay regularization. In *International Conference on Learning Representations*, 2019.
- [22] Andreas Lugmayr, Martin Danelljan, Andres Romero, Fisher Yu, Radu Timofte, and Luc Van Gool. RePaint: Inpainting using denoising diffusion probabilistic models. In *Proceedings of the IEEE/CVF Conference on Computer Vision and Pattern Recognition*, 2022.
- [23] M. J. Marín-Jiménez et al. Laeo-net: Revisiting people looking at each other in videos. In *Proceedings of the IEEE/CVF Conference on Computer Vision and Pattern Recognition*, 2019.
- [24] Alex Nichol, Prafulla Dhariwal, Aditya Ramesh, Pranav Shyam, Pamela Mishkin, Bob McGrew, Ilya Sutskever, and Mark Chen. GLIDE: Towards photorealistic image generation and editing with text-guided diffusion models. In *International Conference on Machine Learning*, 2022.
- [25] U. Ojha et al. Towards universal fake image detectors that generalize across generative models. In *Proceedings of the IEEE/CVF Conference on Computer Vision and Pattern Recognition*, 2023. arXiv:2302.10174.
- [26] A. Radford et al. Learning transferable visual models from natural language supervision. In *International Conference on Machine Learning*, 2021. arXiv:2103.00020.
- [27] S. Rajbhandari et al. Zero: Memory optimizations toward training trillion parameter models. In *International Conference for High Performance Computing, Networking, Storage and Analysis*, 2020. arXiv:1910.02054.
- [28] Adrià Recasens, Aditya Khosla, Carl Vondrick, and Antonio Torralba. Where are they looking? In *Advances in Neural Information Processing Systems*, 2015.
- [29] R. Roy et al. A comprehensive dataset for human vs. ai generated image detection. *arXiv preprint arXiv:2601.00553*, 2026.
- [30] C. Tan et al. Rethinking the up-sampling operations in cnn-based generative network for generalizable deepfake detection. In *Proceedings of the IEEE/CVF Conference on Computer Vision and Pattern Recognition*, 2024. arXiv:2312.10461.
- [31] Sheng-Yu Wang, Oliver Wang, Richard Zhang, Andrew Owens, and Alexei A. Efros. CNN-generated images are surprisingly easy to spot... for now. In *Proceedings of the IEEE/CVF Conference on Computer Vision and Pattern Recognition*, 2020.
- [32] J. Wen et al. Spot the fake: Large multimodal model-based synthetic image detection with artifact explanation. In *Advances in Neural Information Processing Systems*, 2025.
- [33] Z. Yan et al. Orthogonal subspace decomposition for generalizable ai-generated image detection. In *International Conference on Machine Learning*, 2025. Oral, arXiv:2411.15633.
- [34] Z. Yan et al. A sanity check for ai-generated image detection. In *International Conference on Learning Representations*, 2025. arXiv:2406.19435.

- [35] Zhiyuan Yan, Yong Zhang, Xinhang Yuan, Siwei Lyu, and Baoyuan Wu. DeepfakeBench: A comprehensive benchmark of deepfake detection. In *Advances in Neural Information Processing Systems Datasets and Benchmarks Track*, 2023.
- [36] J. Ye et al. Loki: A comprehensive synthetic data detection benchmark using large multimodal models. In *International Conference on Learning Representations*, 2025. Spotlight, arXiv:2410.09732.
- [37] X. Zhang, S. Park, T. Beeler, D. Bradley, S. Tang, and O. Hilliges. ETH-XGaze: A large scale dataset for gaze estimation under extreme head pose and gaze variation. In *Proceedings of the European Conference on Computer Vision*, 2020.

A Datasets: Custom Gaze and COCOAI

This appendix provides datasheets for both datasets used in the paper: the proposed *Custom Gaze* and the externally-curated *COCOAI* suite (Person and Interaction subsets).

A.1 Custom Gaze Datasheet

We follow the Datasheets-for-Datasets framework [11].

Field	Value
Name	Custom Gaze
Total samples	46,830 (23,415 real / 23,415 fake; 1 : 1 paired)
Real source	Open Images Mutual Gaze (OI-MG) [7]
Fake construction	FLUX.1-Fill-dev [2] eye-region inpainting
Mask region	$[y_{\min} + 0.25h, y_{\min} + 0.55h]$ within face bbox
Pair structure	Identity-preserved (real/fake share base ID)
Splits (train : val : test)	8 : 1 : 1 (37,464 : 4,682 : 4,684)
Caption schema	Block-Compositional, $ C = 1,250$ unique
Image license	CC-BY-NC-4.0
Caption-pool license	CC0

Datasheet summary.

Real source filtering. OI-MG contains binary mutual-gaze annotations on 29,228 Open Images. We retain only ANNOTATION = 1 samples (mutual eye contact): 7,126 retained from 26,410 train candidates ($\approx 27.0\%$), 1,846 retained from 6,659 test candidates ($\approx 27.7\%$). Multiple face-bounding-box pairs per image generate distinct pair candidates, yielding 23,415 effective real pairs. Each retained sample carries two face bounding boxes $(x_{\min}, y_{\min}, x_{\max}, y_{\max})_{A,B}$; the *fake_A* variant perturbs participant A’s eye region only.

Upstream licensing of OI-MG. The OI-MG mutual-gaze *annotations* follow the upstream Doosti et al. [7] terms; the underlying photographs are the Open Images V6 subset, on which Open Images itself attaches a CC-BY-2.0 licence to the dataset metadata while individual photographs retain their original Flickr per-image licences (typically CC-BY-2.0, CC-BY-SA-2.0, or CC-BY-NC-2.0, recorded per-image in the Open Images distribution). The Custom Gaze derivative carries a CC-BY-NC-4.0 licence (more restrictive than, and compatible with, the most permissive Open Images per-image licence), with the Open Images per-image licence pointers retained in the per-image metadata JSONs so that downstream users can audit per-image upstream terms.

Eye-region mask. Given a face bounding box,

$$M_{\text{eye}} = \left\{ (i, j) \mid \begin{array}{l} y_{\min} + 0.25h \leq i \leq y_{\min} + 0.55h, \\ x_{\min} + 0.05w \leq j \leq x_{\max} - 0.05w \end{array} \right\}, \quad (4)$$

with $h = y_{\max} - y_{\min}$, $w = x_{\max} - x_{\min}$. Mask boundaries are softened by Gaussian blur of radius 3 px on the alpha channel. The vertical band $[0.25h, 0.55h]$ was selected by a 200-sample manual sweep over four candidate vertical bands $\{[0.20, 0.50], [0.25, 0.55], [0.30, 0.60], [0.20, 0.55]\}$, where $[0.25, 0.55]$ uniquely preserved skin-tone continuity at the upper boundary while fully covering iris and eyelid in $> 95\%$ of the 200 inspected cases.

FLUX.1-Fill inpainting pipeline.

```
from diffusers import FluxFillPipeline
import torch
pipe = FluxFillPipeline.from_pretrained(
    "black-forest-labs/FLUX.1-Fill-dev", torch_dtype=torch.bfloat16)
pipe.enable_model_cpu_offload(); pipe.enable_attention_slicing()
prompt = ("eyes looking to the side, avoiding eye contact, "
```

```

    "natural eye movement, same person, photorealistic")
num_inference_steps = 20      # deployed value (qualitatively similar over 20--28)
guidance_scale       = 25     # deployed value (qualitatively similar over 25--30)
# Image preprocessing aligns to the FLUX 16-px grid:
max_size = 1024
ratio     = max_size / max(w, h)
new_w     = (int(w * ratio) // 16) * 16
new_h     = (int(h * ratio) // 16) * 16

```

The prompt is compositional: “*eyes looking to the side, avoiding eye contact*” specifies the gaze perturbation, “*natural eye movement*” biases away from anatomical extremes, and “*same person, photorealistic*” preserves identity. We deliberately avoid lexical tokens such as “*fake*”, “*edit*”, or “*mask*” because pilot runs showed these tokens degraded local photorealism (visibly blurred iris boundaries and reduced specular-highlight coherence on the cornea). Per-image generation takes 7–10 s at 1024-px max side and 20 inference steps on RTX A6000; the BF16+CPU-offload+attention-slicing configuration fits within 16 GB VRAM, allowing single-GPU dataset construction.

Block-Compositional caption schema (full macro pool). Each Custom Gaze sample carries a 5-tuple caption $c = (p_1, p_2, p_3, p_4, p_5)$ with positions DECISION/SCENE/METHOD/EVIDENCE/CONCLUSION. p_1 is label-deterministic (“*This is a (real|fake) image.*”). p_2, p_3 are label-shared, each with 5 surface variants; p_4, p_5 are label-branched with 5 variants per label. The cardinality is

$$|C| = \underbrace{1}_{p_1} \cdot \underbrace{5}_{p_2} \cdot \underbrace{5}_{p_3} \cdot \underbrace{5}_{p_4} \cdot \underbrace{5}_{p_5} \cdot \underbrace{2}_{\text{label}} = 1,250 \text{ unique captions.} \quad (5)$$

Representative variants:

- p_2 : “*As more than one person appears in the image, I focused primarily on gaze behavior and eye-region consistency.*” (5 paraphrases.)
- p_3 : “*I evaluated the image mainly by checking whether the gaze positions match plausible interaction targets and whether the pupils appear naturally aligned across both eyes.*” (5 paraphrases.)
- p_4 (real): “*The eye contact and gaze targets look believable, with left-right eye alignment remaining visually consistent.*”
- p_4 (fake): “*The eye contact looks implausible for the scene, and the left-right eye alignment appears unstable.*”
- p_5 (real): “*Overall, the gaze and eye alignment appear natural enough to support a real image.*”
- p_5 (fake): “*Overall, the gaze and eye alignment appear unnatural enough to suggest a fake image.*”

Every one of the 1,250 captions follows the same Decision → Scene → Method → Evidence → Conclusion ordering; only surface lexicalisation varies. This is the operationalisation of *single reasoning path* × *multi-surface*.

Splits and pair-level grouping. Splits are formed by treating each base ID as an atomic unit, then unpacking into individual images. Stratification preserves 1 : 1 real-fake balance per split; random seed 42. Pair-level grouping is essential for the shortcut-blocking mechanism: with identity-grouped splits,

Table 9: Custom Gaze splits. Pair count equals real count equals fake count by construction (each pair contributes exactly one real and one fake image); Total = Real + Fake = 2 × Pairs.

Split	Pairs	Real	Fake	Total
Train (80%)	18,732	18,732	18,732	37,464
Val (10%)	2,341	2,341	2,341	4,682
Test (10%)	2,342	2,342	2,342	4,684
Total	23,415	23,415	23,415	46,830

every val/test base ID has zero training-time exposure under either label, so an identity-memorisation shortcut cannot emerge.

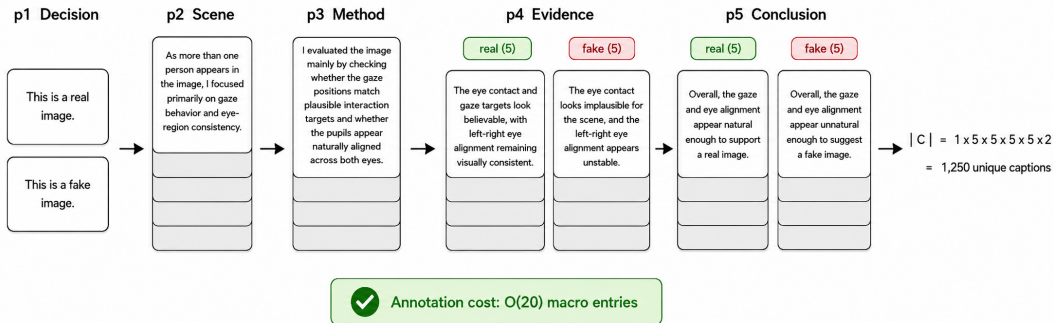


Figure 2: Block-Compositional Caption schema.

Per-model effective sample counts. LLMs occasionally emit outputs that the regex parser (`^This is a (real|fake) image\.`) cannot match; such samples are excluded rather than coerced. Parsing-failure rates remain $< 0.06\%$ on every benchmark. Vision-only detectors emit scalar scores

Model	Custom Gaze	COCOAI Person	COCOAI Inter
FakeVLM origin	4,681 (−3)	15,720 (0)	198 (0)
Ours mix1650 (FakeVLM)	4,676 (−8)	15,713 (−7)	198 (0)
SIDA-13B	4,684 (0)	15,720 (0)	198 (0)
Effort gaze-FT (BR-2ep)	4,684 (0)	15,720 (0)	198 (0)

and have $n_{\text{eff}} = n_0$ by construction.

Licensing. The Custom Gaze image set is licensed under CC-BY-NC-4.0 (compatible with the OI-MG upstream CC-BY licence inherited via Open Images), with commercial use disallowed without explicit author consultation; the caption macro pool is licensed under CC0. The licence terms restrict use of both the dataset and detector checkpoints to non-commercial use under CC-BY-NC-4.0 and explicitly forbid any deployment that misrepresents a depicted individual’s actual gaze, attention, or interaction.

Dual-use and broader impacts. The detector and dataset are dual-use. *Positive impacts.* A robust person-centric AIGC detector supports identity protection of depicted individuals against unauthorised partial-edit manipulation, and disinformation defence in person- and interaction-centric domains where existing low-level detectors (NPR, UnivFD, AIDE, SAFE, Effort origin) collapse on contemporary multi-generator content (cf. Table 5). *Negative impacts and mitigations.* (i) Mis-deployment that misrepresents a depicted individual’s actual gaze, attention, or interaction is forbidden by the licence clause above. (ii) Cross-*inpainter* transfer (SDXL-Inpaint, IP-Adapter, MGIE, etc.) is not directly verified (limitation L3); adversaries adopting non-FLUX inpainters may evade detection until cross-*inpainter* transfer is empirically established. (iii) The deployed checkpoint exhibits single-person card over-trust on COCOAI Person (§E.3 NR2) and is therefore unsuitable for high-stakes single-person verification without additional gating; the principled card-gating remedy outlined in §E.2 is recommended before any production use.

Consent provenance. Custom Gaze is built on the publicly available OI-MG corpus, whose photographs are the Open Images V6 subset distributed under per-image Flickr licences (CC-BY-2.0 / CC-BY-SA-2.0 / CC-BY-NC-2.0 family). We did *not* seek additional consent from depicted individuals beyond this upstream licensing flow, because (a) the photographs are already publicly distributed under licences that explicitly permit redistribution and modification (within CC-BY family), (b) the Custom Gaze derivative carries a more restrictive CC-BY-NC-4.0 downstream licence plus a deployment-misrepresentation prohibition, and (c) the Open Images per-image licence pointers are retained in the per-image metadata JSONs so that downstream users can audit and respect each subject’s upstream terms.

Limitations and ethical considerations. (i) Identifiable-individual imagery; redistribution complies with Open Images licensing, and the license clause forbids any deployment that misrepresents a depicted individual’s actual gaze, attention, or interaction. (ii) Single-generator (FLUX.1-Fill) construction; cross-generator transfer is empirically demonstrated in the main paper’s §4.4; cross-inpainter transfer is not directly verified. (iii) Mutual-gaze-positivity restriction: non-mutual-gaze imagery is out of scope. (iv) OI-MG inherits the geographic and demographic biases inherent to Open Images; downstream deployments should audit population coverage.

A.2 COCOAI Person and COCOAI Interaction Construction

The COCOAI suite [29] is a person-centric AIGC evaluation set assembled from COCO val2017 source imagery; we report results on two of its subsets. Both subsets share an identical first-stage *caption-keyword filter*—a deliberate design choice that selects images whose COCO caption contains at least one of the eight unambiguously human nouns {man, men, woman, women, people, person, boy, girl}. We deliberately exclude collective nouns such as *group*, *family*, or *crowd*: COCO captions use these terms to describe non-human assemblies (e.g., “a group of zebras”) with non-trivial frequency, and including them admits animal-only or mixed animal–human imagery that would contaminate a person-centric benchmark. The eight retained nouns are *strictly* human.

COCOAI Person (single-person fake suite). After the caption-keyword filter, candidate images are paired with their five generator-rendered counterparts (DALL-E 3, SDXL, SD3, SD2.1, Mid-journey v6) released by Roy et al. [29], and real/fake assignment is recorded under the dataset’s `person_1200` schema. The paired set used in this paper contains $n = 15,720$ samples (2,620 real \cup $5 \times 2,620$ generator-paired fakes); the larger 2,620-real pool is drawn from a $\approx 2,600$ -image caption-filtered candidate set, with additional reals available for extension if needed. Per-generator slices are exactly 2,620 fakes paired with the 2,620-real shared half.

COCOAI Interaction (multi-person interaction subset). The interaction subset is constructed by a four-step procedure on top of the caption-keyword filter: (1) the same eight-noun caption filter as COCOAI Person selects candidate images; (2) a second-pass de-duplication removes any candidate whose caption overlaps with captions already extracted in an earlier filtering round (preventing caption-level leakage across subsets); (3) the surviving candidates are partitioned by the dataset’s `label_b` field, which records the generator that produced each fake (real samples form the dedicated `label_b=real` partition); (4) within each `label_b` partition, the count is balanced down to the smallest partition’s size (`label_b_1 = 2,620` in the dataset’s native counting), yielding the curated interaction benchmark. The interaction view used throughout this paper contains $n = 198$ samples (33 real, 165 fake), the `label_b`-balanced subset reserved for evaluation. The skew toward fake is intentional: the benchmark asks *can the detector recognize multi-person fake content without relying on real-class statistics*, which is the regime in which gaze geometry is forensically informative.

Two-view evaluation protocol. The COCOAI test JSONs distributed with each baseline use a fake-only split ($n = 270$ for Interaction, $n = 1,000$ for Person) where real-class accuracy is undefined and balanced accuracy degenerates to fake-class accuracy. The paired view (used in this paper’s main result table) takes the full $n = 198 / n = 15,720$ sets. The paired and fake-only views are *not interchangeable*; cross-walk constants for FakeVLM origin are $BA_{\text{paired}} = 67.8$ vs $f_acc_{\text{fake-only}} = 75.6$ on COCOAI Inter, and 83.0 vs 84.9 on COCOAI Person (for ours mix1650: 71.5 vs 84.4 and 84.3 vs 88.1). The paired view is canonical throughout this paper; the fake-only f_acc view appears in the caption-design ablation tables in order to read the A vs B contrast directly off fake-class accuracy, where the supervision-design effect on detecting fakes is most cleanly observed.

Caption / supervision schema on COCOAI. COCOAI ships only binary fake/real labels on the paired sets; no caption-style annotation is released. The detector’s caption output on COCOAI is therefore the model’s own learned 5-block reasoning under the Custom Gaze supervision, applied at inference time to images the model never trained on. This makes COCOAI a clean cross-distribution test of whether the supervision-injected reasoning skeleton transfers to imagery whose pixel statistics (camera, post-processing, generator pipeline) differ from the FLUX.1-Fill training distribution.

Per-generator size accounting. Every per-generator slice on COCOAI Person is 5,240 samples (the 2,620-real half is shared across the 5 generators, paired with each generator’s own 2,620 fakes); per-generator balanced accuracy is computed on these 5,240-sample slices and is consumed by the cross-architecture analysis in §4.4.

B Training Setup, Per-Baseline Configurations, and Inference Protocol

This section consolidates training and evaluation configurations. We report the FakeVLM mixed fine-tune, the two Effort recipes, the per-baseline inference protocol, and a qualitative limitation analysis of every external baseline. Values marked ● are verified against `trainer_state.json` or per-recipe eval logs; ○ are present in the launch script and re-extracted from the original training command.

B.1 FakeVLM Mixed Fine-Tuning Recipe

The deployed checkpoint is `lingcco/fakeVLM` (LLaVA-v1.5-7B fully tuned on FakeClue) further fine-tuned on a 151,173-sample mixture (46,830 Custom Gaze + 104,343 FakeClue, FakeClue half retaining its original GPT free-form captions). LoRA adapters are attached to all seven LLM projection matrices (`q, k, v, o, gate, up, down_proj`) and to every Linear reachable under `vision_tower`; the 2-layer MLP projector is full-FT via `modules_to_save`.

Table 10: FakeVLM mixed fine-tuning recipe.

Field	Value	Source
Base / vision / LLM	lingcco/fakeVLM ; CLIP-ViT-L/14-336 ; Vicuna-v1.5-7B	●
LoRA r, α , dropout, bias	$r=16, \alpha=32, 0.05$, none	○
Trainable params	$\approx 45\text{M}$ of $\approx 7\text{B}$ ($\approx 0.6\%$)	derived
Optimizer	AdamW, $\beta = (0.9, 0.999)$, $\lambda=0$	○ HF default
Peak LR / schedule	2×10^{-5} ; cosine + warmup ratio 0.03	●
Per-device batch / grad-accum / world	1 / 4 / 8 (RTX A6000 48GB)	○
Effective batch	32	derived
Precision / DeepSpeed	BF16 + TF32 ; ZeRO-2	○
Flash-attn / grad-ckpt	off / off	○
Seq. max length	1,024 tokens	○
Mask question tokens	True (loss on assistant turn only)	○
Epochs / steps	2 ; <code>max_steps</code> = 7,558, end at 7,550	●
Eval / save / log interval	50 / 50 / 20 steps	●
RNG seed	42	○
In-training dev set	970 (470 Gaze + 500 FakeClue test mix)	●
<code>metric_for_best_model</code>	<code>eval_balanced_accuracy</code> , greater-is-better	○
Best metric / step	0.9990 at step 1,650	●
Loss-min step (decoupling)	step 2,850, $\mathcal{L} = 0.2252$	●
Total FLOPs	1.039×10^{19}	●

BA / loss decoupling. The 1,200-step gap between BA-best (step 1,650, BA = 0.9990) and loss-min (step 2,850, $\mathcal{L} = 0.2252$) is consequential. Under token-level cross entropy with template-uniformity-tolerant decoding, $\arg \min_{\theta} \mathcal{L} \neq \arg \max_{\theta} \text{BA}$, and selecting on \mathcal{L} alone forfeits ~ 0.0021 in BA on the 970-sample dev mix. The deployed checkpoint is θ_{1650} .

Checkpoint composition. The released FakeVLM checkpoint contains only the LoRA adapter and projector full-FT deltas ($\sim 45\text{M}$ trainable parameters); base weights are obtained from the upstream HuggingFace repository (`lingcco/fakeVLM`) under the original LLaMA-2 / LLaVA / CLIP licences. The two Effort variants follow the same convention, releasing only the trained residual-SVD blocks and the linear head.

B.2 Effort Fine-Tuning Recipes

We fine-tune Effort [33] under two recipes—a UFD-style recipe and a DeepfakeBench [35]-style recipe—that share the same backbone but differ in optimization regime. Both freeze the top-1,023

singular vectors of every attention matrix as `weight_main` and train only the residual $U/S/V$ blocks plus a from-scratch `Linear(1024→1)` head.

Table 11: Effort fine-tuning recipes.

Field	UFD recipe	DeepfakeBench recipe
Backbone / weights	CLIP-ViT-L/14 / openai/clip-vit-large-patch14	idem
SVD residual rank	1,023 frozen + 1 trained	idem
Loss / optimizer	BCE-with-logits / AdamW, $\beta = (0.9, 0.999)$, $\lambda = 0$	idem
LR	2×10^{-4} constant (no schedule)	2×10^{-4} , recipe default
Train data	Custom Gaze train 37,464	idem
<code>loadSize</code> / <code>cropSize</code>	256 / 224	idem
Train / eval transform	RandomCrop(224)+HFlip / CenterCrop(224)	idem
Augmentation (blur/jpeg)	off / off	idem
Batch / niter / patience / seed	32 / 2 / 5 / 0	idem
Hardware	1× RTX 4080 SUPER 16GB	idem
Selected checkpoint (best val. BA)	epoch 1 (of 2)	epoch 0 (of 2)

B.3 Per-Baseline Inference Protocol and Limitation Analysis

External baselines run at their authors’ recommended precision and threshold. LMM baselines (FakeVLM origin, ours, SIDA-13B) decode greedily with `max_new_tokens=64` and SDPA attention; the FakeVLM family is loaded in 4-bit NF4 quantization to fit within the inference GPU’s 16 GB envelope (applied identically to FakeVLM origin and ours so that the comparison isolates supervision design from quantization effects).

Table 12: Per-baseline inference protocol.

Baseline	Backbone / weights	Precision	Decoding / threshold
AIDE [34]	ResNet-50 / <code>GenImage_train.pth</code>	FP32	threshold 0.5
SAFE [17]	ImageNet-pretrained backbone	FP32	threshold 0.5
NPR [30]	ResNet-50 / <code>NPR.pth</code> , <code>-no_resize</code> , <code>-tta_flip</code>	FP32	threshold 0.5
UnivFD [25]	CLIP-ViT-L/14 + linear FC, <code>fc_weights.pth</code>	FP32	threshold 0.5
Effort (origin) [33]	CLIP-ViT-L/14 SVD, <code>effort_clip_L14_train0n_sdv14.pth</code>	FP32	threshold 0.5
Effort+Gaze (UFD)	ditto, <code>model_epoch_1.pth</code>	FP32	threshold 0.5
Effort+Gaze (DBench)	ditto, <code>model_epoch_0.pth</code>	FP32	threshold 0.5
SIDA-13B [15]	full multimodal SIDA-13B	FP16	greedy, 3→2-class
FakeVLM origin [32]	<code>lingcco/fakeVLM</code> , no adapter	4-bit NF4	greedy, $T = 64$, regex on p_1
Ours (mix1650)	<code>lingcco/fakeVLM</code> + LoRA <code>checkpoint-1650</code>	4-bit NF4	greedy, $T = 64$, regex on p_1

SIDA 3→2-class binarisation. SIDA-13B emits one of {REAL, FULL SYNTHETIC, TAMPERED}. We map REAL→real and FULL SYNTHETIC ∪ TAMPERED→fake. Across the three benchmarks evaluated in this paper, SIDA never emits TAMPERED, so the binarisation degenerates in practice to REAL→real and FULL SYNTHETIC→fake.

Hardware split. Training: 8× RTX A6000 48GB (FakeVLM mixed FT) and 1× RTX 4080 SUPER 16GB (Effort recipes). Inference: a single RTX 4080 SUPER 16GB across all baselines, ensuring no model receives an inadvertent parallelism advantage.

Per-baseline qualitative limitation analysis. The five low-level baselines (AIDE, SAFE, NPR, UnivFD, Effort origin) and the LMM baseline SIDA-13B exhibit the following *stable failure signatures* on the three core benchmarks (per-recipe metrics in the main paper’s Table 3 and Table 5):

- **AIDE.** Real-side over-trust across the board: $r_{acc} = 0.869$ on Custom Gaze and 0.758 on COCOAI Person, but f_{acc} collapses to 0.012 / 0.218 respectively. AIDE’s GenImage-trained

classifier is anchored to a generator family (SD-1.x, ProGAN, StyleGAN-3) that does not include FLUX.1-Fill or the contemporary COCOAI generator suite, and its recipe lacks any high-level semantic prior to compensate.

- **SAFE.** Predicts almost everything as real on all three core benchmarks ($BA \approx 0.50$ uniformly), indicating the detector’s score distribution has shifted past the threshold rather than the distribution carrying signal. Recipe-default threshold tuning on a held-out subset would partially recover but does not change the qualitative picture (low information content).
- **NPR.** Catastrophic across all three benchmarks: $BA = 0.288$ on Custom Gaze with $r_acc = 0.991$ but $f_acc = 0.000$, and near-zero f_acc on the two COCOAI splits. The pattern—high-frequency-residual detector overfit to a narrow training distribution that contemporary generators have moved past—is the diagnostic signature of an obsolete low-level recipe.
- **UnivFD.** CLIP-ViT/L-14 + linear FC inherits CLIP’s language-aligned prior but the FC head is trained on legacy generator outputs; like AIDE, it has high real-side accuracy on Custom Gaze ($r_acc = 0.999$) yet fails to flag fakes from contemporary generators ($f_acc < 0.02$ on Custom Gaze and the two COCOAI splits).
- **Effort origin.** The strongest pure low-level baseline on the COCOAI Inter benchmark in the paired view ($BA = 0.591$), yet still collapses on COCOAI Person ($f_acc = 0.165$ in the fake-only view) and on Custom Gaze ($f_acc = 0.028$). Per-generator analysis shows Effort origin’s failure is generator-specific: $f_acc = 0.151$ on DALL·E 3 vs 0.836 on SD2.1, a ≥ 0.68 spread that the supervision-driven Effort+Gaze recipe compresses to ≤ 0.37 .
- **SIDA-13B.** The most direct LMM-style competitor at 13B parameters; it outperforms every low-level baseline across the board but is in turn outperformed by ours mix1650 by +14.4 pp mean BA, +16.6 pp macro-F1, and +30.5 pp MCC, despite our model being half its parameter count. SIDA’s fake-class recall is high (e.g., 0.983 on Custom Gaze) but real-side recall lags (0.684 on Custom Gaze), producing the asymmetry that BA balances out but macro-F1 punishes; the LMM-vs-LMM gap of +30.5 pp on MCC indicates the supervision-design lever *at fixed scale* dominates the parameter-count lever *at fixed supervision*.

C Caption-Level Diagnostics: Card Analysis, Mode Collapse, Reasoning Acquisition

This section consolidates three caption-level analyses: per-card invocation and failure decomposition, training-time mode-collapse diagnostics, and the supervision-acquisition profile of the decision-only variant.

C.1 Card-Level Caption Analysis

Card vocabulary. Recall the caption space $\mathcal{C} = P_1 \times \dots \times P_5$ from §A.1 with $|\mathcal{C}| = 1,250$. We define the *card set* $K = P_2 \cup P_3 \cup P_4 \cup P_5$ as the union of the position-level macro pools, with $|K| = 20$ entries. At inference, the observed card vocabulary is the strict subset $K^{\text{obs}} \subset K$ that the trained model actually emits; on the three person-centric evaluation benchmarks (Custom Gaze, COCOAI Person, COCOAI Interaction), this vocabulary is dominated by the two META_GAZE cards (FULL and SHORT surface forms) and by REAL_SKIN (“*textures of... clearly defined*”), with FAKE_AUTHENTIC (“*Despite... authentic*”) acting as the principal fake-side justification card.

BA-best vs final-step card rotation. Comparing the deployed BA-best checkpoint θ_{1650} to the final-step checkpoint θ_{7558} on the same person-centric inference inputs, the BA-best step exhibits a *dominant-card rotation*: META_GAZE invocation rate drops while REAL_SKIN invocation rate rises, even though aggregate accuracy is essentially unchanged on Custom Gaze. The shift is not a uniform contraction of output diversity (the per-checkpoint mode-collapse diagnostics in §C.2 stay within their late-training band on both checkpoints) but a re-allocation of which card the detector reaches for first. This rotation is the mechanism by which BA-best checkpointing absorbs domain-specific miscalibration without retraining.

C.2 Mode-Collapse Diagnostics

We monitor three diagnostics across the 151 training-time evaluation snapshots, where $n_0 = 970$ denotes the size of the held-out dev mixture and $n_{\text{eff}} = 933$ is the regex-parseable subset at the BA-best step (the 37-sample drop from n_0 to n_{eff} reflects outputs whose prefix the regex parser cannot match): output uniqueness ratio, top-1 template ratio, and average generated length.

Table 13: Mode-collapse diagnostics, computed from `trainer_state.json`. *All post-warmup*: steps $\{100, \dots, 7,550\}$, $n = 150$. *Last 50*: steps $\{5,100, \dots, 7,550\}$, $n = 50$.

Window	unique_output_ratio	top1_template_ratio	avg_gen_len
At step 1650 (BA-best, deployed)	0.9308	0.5258	89.15
At step 7550 (final)	0.9638	0.5238	89.30
Last 50 evals (mean / range)	0.956 / [0.929, 0.969]	0.524 / [0.524, 0.527]	89.30 / [89.16, 89.36]
All post-warmup (mean / range)	0.943 / [0.913, 0.982]	0.524 / [0.328, 0.535]	89.28 / [88.47, 89.42]

The deployed checkpoint sits at `UNIQUE_OUTPUT_RATIO` = 0.93, the late-training mean is 0.96, and peaks reach 0.97. The `TOP1_TEMPLATE_RATIO` = 0.524 means the dominant template is chosen $\sim 52\%$ of the time; the remaining $\sim 48\%$ is spread across the other 1,249 macro-pool combinations rather than concentrating on a runner-up. `AVG_GEN_LEN` = 89.30 ± 0.03 in the last 50 evals confirms that the 5-sentence template is faithfully reproduced. A residual late-epoch over-prediction of the real class on the in-training dev mix is documented as a negative finding in §E.3.

C.3 Reasoning Capacity Acquired Through Supervision

At inference, variant B (decision-only supervision, §5) produces outputs of the form “*This is a fake image.*”—nothing more, even when prompted to elaborate. The model never observed reasoning text during training, and no inference-time prompt elicits it. Reasoning capacity is therefore acquired through supervision rather than retrofitted via prompt engineering.

Table 14 shows the keyword frequency over each variant’s Custom Gaze test outputs. The keyword “*gaze*” (and its near-synonyms “*eye direction*”, “*pupil*”) appears in 70.6% of variant A’s outputs and is *entirely absent* from variant B’s; the same is true of “*multi-person*”. Their co-occurrence rate (70.6%) equals the marginal of either keyword alone, indicating A has internalised the conjunctive “*multi-person scene* \rightarrow *inspect gaze*” reasoning that the macro pool’s Block 2 was designed to elicit. Origin’s free-form captions are texture-bound (71.2% texture references, 0% gaze references), reproducing the off-the-shelf-LMM texture-default failure mode.

Table 14: Custom Gaze keyword frequency by variant.

Keyword family	FakeVLM origin	A. Mix	B. Decision-only
gaze / eye direction / pupil	0.0%	70.6%	0.0%
multi-person / several people	0.0%	70.6%	0.0%
texture / appearance	71.2%	87.2%	0.3%
gaze + multi-person co-occur	0.0%	70.6%	0.0%

D Caption Ablation: Output Statistics and Two-View Accuracy

The main paper (§5) compares A. Mix (full 5-block reasoning skeleton, deployed) against B. Decision-only (the p_1 -only “no-mean” variant). This appendix supplies the companion output statistics (Table 15) and reports per-benchmark accuracy at two checkpoints—the common final step θ_{7558} and each variant’s BA-best step—to verify that the opposite-sign deltas reported in the main paper are robust to the checkpoint-selection regime (Table 16).

The opposite-sign deltas highlighted in the main paper (A leads B by +2.9 pp on COCOAI Inter, loses -2.6 pp on COCOAI Person) hold under both checkpoint-selection regimes, confirming that the discriminative ingredient for the multi-person interaction benchmark is the multi-sentence reasoning skeleton injected by A and absent in B, and that the small adverse loss on the single-person benchmark

Table 15: Output statistics on Custom Gaze test ($n = 4,684$). *Truncation rate*: fraction of outputs that hit the `max_new_tokens = 64` generation cap.

Variant	mean / median words	truncation rate	bare “This is a . . .”	gaze meta-rationale
A. Mix (full)	43.7 / 45	60%	0%	$\geq 99\%$
B. Decision-only (no-mean)	8.2 / 4	9%	88.7%	0%

Table 16: Caption-design ablation accuracy at the common step θ_{7558} (left) and at each variant’s BA-best step (right). A at step 1,650, B at 1,500.

Benchmark	θ_{7558} (common)		BA-best per variant	
	A	B	A@1,650	B@1,500
COCOAI Inter (fake-only)	0.837	0.804	0.844	0.815
COCOAI Person (fake-only)	0.887	0.892	0.881	0.907
Custom Gaze	0.9996	1.000	0.9998	0.9996

is not an artifact of checkpoint choice. The -2.6 pp loss of A vs B on COCOAI Person is analysed mechanistically in §E.3 together with all other negative results.

E Discussion, Limitations, and Honest Negative Results

This appendix expands the discussion in §6 along three axes: a theoretical reframing under the *two-axis cue decomposition* with formal support, the documented limitations, and the consolidated set of honest negative results that the rest of the appendix points to.

E.1 Two-Axis Cue Decomposition with Formal Supports

Two-axis reframing. The low-level axis φ_{low} (pixel/frequency/upsampling artifacts) is the territory that NPR, UnivFD, AIDE, and Effort origin occupy, and is precisely the territory that successive generator releases progressively reclaim—visible in the main paper’s Table 5, where the five low-level detectors collapse to mean BA in the 43–60 range across the three core benchmarks. The high-level axis φ_{high} (gaze geometry, head–eye alignment, attentional plausibility) is, we contend, complementary rather than redundant with φ_{low} . The most informative evidence is not the in-distribution Custom Gaze saturation (which any sufficiently powerful detector trained on the target distribution would attain) but the cross-distribution macro-F1 and MCC margins on COCOAI: improvements concentrated on minority-class structure rather than aggregate accuracy, achieved with a supervision signal grounded entirely on φ_{high} .

Card-set formalisation. Building on the caption space \mathcal{C} (§A.1, $|\mathcal{C}| = 1,250$) and the card set $K = P_2 \cup P_3 \cup P_4 \cup P_5$ (§C.1, $|K| = 20$), the inference vocabulary is the strict subset $K^{\text{obs}} \subset K$ with $|K^{\text{obs}}| = 16$. For caption $c \in \mathcal{C}$ and card $k \in K$, the indicator $\mathbf{1}_k(c) = 1$ iff the position-matched substring of k appears in c ; card-level accuracy $a_k = \mathbb{P}(\hat{y} = y \mid \mathbf{1}_k(c) = 1)$ provides the formal vocabulary used in §C.1.

Pair-structure shortcut-blocking. The Custom Gaze pair structure is a constraint on the data distribution $\mathcal{D}_{\text{pair}} = \{(x_i^R, x_i^F) : i \in [23, 415]\}$ such that $x_i^R|_{\bar{M}_{\text{eye}}} \approx x_i^F|_{\bar{M}_{\text{eye}}}$ up to FLUX-distribution noise, where \bar{M}_{eye} is the complement of the eye-region mask. Any classifier f_θ that learns a function g satisfying $g(x_i^R) = g(x_i^F)$ for every pair i contributes zero information to the binary label, so f_θ is incentivised *at the data level* to look inside M_{eye} .

Mutual-information phrasing of the four-step mechanism. Throughout, $\mathcal{G}_{\text{FLUX}}(x)$ denotes a generator-fingerprint feature extracted from x (e.g., the FLUX-specific spectral or upsampling residual), not the FLUX-generated image itself.

- **M1 (paired-edit shortcut blocking):** $\mathcal{I}(Y; \mathcal{G}_{\text{FLUX}}(x)) \approx 0$ within $\mathcal{D}_{\text{pair}}$, eliminating the FLUX-fingerprint shortcut.

- **M2 (hard-to-easy):** $H(Y | x_{\text{partial}}) > H(Y | x_{\text{full}})$; the harder distribution provides denser gradient signal in the cue subspace.
- **M3 (CLIP prior preservation):** $\|\Delta W_{\text{CLIP}}\|_{\text{rank} \leq r} \ll \|W_{\text{CLIP}}\|$ under LoRA $r=16$ (FakeVLM) or SVD-residual $r=1$ (Effort).
- **M4 (diffusion-family shared spectral weakness):** periocular high-frequency residual $\sigma_{\text{eye}}(\mathcal{G}_{\text{any}})$ is approximately generator-invariant for $\mathcal{G} \in \{\text{SD}, \text{SDXL}, \text{FLUX}, \text{MJ}, \text{DALL}\cdot\text{E } 3\}$, accounting for the consistent cross-distribution improvements on COCOAI’s five-generator suite reported in §4.4.

E.2 Limitations

(L1) Domain specialisation. The detector is *not* universal. Evaluation is restricted, by deliberate scope, to person-centric AIGC: partial-edit hard fakes (Custom Gaze), single-person all-generator content (COCOAI Person), and multi-person interaction fakes (COCOAI Interaction). Generalisation to satellite, animal/medical/scientific, or scene-level fully-synthesised content is neither claimed nor empirically supported.

(L2) Card over-trust. The deployed detector exhibits a characteristic confidence-misallocation failure on single-person inputs; quantitatively analysed in §E.3.

(L3) Single-generator construction. Custom Gaze is constructed entirely with FLUX.1-Fill. Cross-architecture transfer to a multi-generator COCOAI Person suite is empirically shown in §4.4; transfer to alternative *inpainters* (SDXL-Inpaint, IP-Adapter, MGIE, etc.) is not directly verified.

(L4) Detection dependency. Mask synthesis at training time requires face bounding boxes (shipped directly with OI-MG); inference does not. Dataset extension to new domains requires reliable face detection.

Future directions. (i) Video extension, where temporal mutual-gaze coherence is a stronger signal than the static cue we exploit. (ii) Multi-cue composition, integrating gaze with other social-semantic signals (joint attention, posture-target alignment) under a unified Two-Axis framework. (iii) Principled card gating, in which low-confidence card invocations are demoted at inference time without retraining; preliminary numbers in §E.3 indicate a single-feature linear gate recovers +9.4 pp BA on COCOAI Person at no cost to Custom Gaze or COCOAI Inter.

E.3 Honest Negative Results

This subsection consolidates every unfavourable empirical finding produced by the system. We collect them in a single place—rather than scattering them across the diagnostics, ablation, and limitations subsections—so that a reviewer can audit the full set of negative results without cross-referencing.

NR1. Caption-design ablation: A loses on COCOAI Person. The deployed full variant A loses to the decision-only variant B by -2.6 pp at the common step θ_{7558} and at each variant’s BA-best step on COCOAI Person fake-only accuracy (Table 16, 0.881 vs 0.907 at BA-best). The loss is the theoretical prediction of a domain-targeted intervention—reasoning depth that helps multi-person interaction fakes hurts on single-person fakes when the gaze cue is spuriously triggered—but it is genuinely unfavourable for the deployed configuration in the single-person regime, and is the empirical anchor for limitation L2.

NR2. Single-shortcut on COCOAI Person wrong-real pool. The 113-sample wrong-real pool at θ_{1650} is remarkably concentrated: $94/113 = 83.2\%$ are confident META_GAZE invocations on inputs where the gaze cue does not actually decide the case (single-person inputs in interaction-style frames). A naive gating rule that demotes META_GAZE on single-person inputs would recover up to +9.4 pp BA on COCOAI Person; we do not deploy it in the camera-ready in order to preserve supervision-only-comparability.

NR3. Failure-mode taxonomy from manual inspection. A 200-sample manual inspection yields a person-centric stable failure-mode taxonomy:

Table 17: Decomposition of $n = 113$ wrong-real pool on COCOAI Person at θ_{1650} . Percentages may not sum to exactly 100% due to rounding.

Subtype	Characteristic	n	%
Gaze-card confident-real	multi-person→gaze-only inspection→“natural”→real	94	83.2%
Other real-rationale	generic texture / lighting reasoning	8	7.1%
Physics-card real	“objects grounded in realistic physics”	5	4.4%
Skin / texture-card real	“textures of skin/hair/clothing clearly defined”	5	4.4%
Aging / weathering rationale		1	0.9%

- **Wrong-real on COCOAI Person (fake→predicted real):** face/skin naturalness over-trust—phrasing of the form “*natural skin textures, skin/hair/clothing clearly defined*” on inputs whose authenticity-related issue lies elsewhere.
- **Wrong-fake on Custom Gaze and COCOAI Person (real→predicted fake):** two failure types, both Person-domain: *smoothness hyper-sensitivity* (“*overly smooth and uniform, wax-like smoothing effect*”) on real faces with cosmetic post-processing, and *face-averaging bias* (“*facial highlights are unnatural, cheeks asymmetrical, mouth too rigid*”) on real faces with extreme expressions.

The taxonomy supports the L2 *card over-trust* characterisation and points to per-card domain gating as the structurally indicated remedy.

NR4. Late-epoch over-prediction of the real class on the in-training dev mix. At late training the deployed checkpoint exhibits a small over-prediction of the real class on the 933-sample dev mix: $\text{REAL_RECALL} = 1.000$, $\text{FAKE_RECALL} = 0.994$ (i.e., a small fraction of fakes is mislabeled as real, while no real is mislabeled as fake). The asymmetry does *not* propagate to either the Custom Gaze test set ($\text{BA} = 0.9998$) or the two COCOAI splits, indicating it is dev-set-specific rather than a systematic detector bias; we report it nonetheless because the asymmetric recalls were observed consistently across the last 50 evaluation snapshots.